PNAS RESEARCH ARTICLE | CELL BIOLOGY

PARG inhibitor sensitivity correlates with accumulation of single-stranded DNA gaps in preclinical models of ovarian cancer

Ramya Ravindranathan[a,b], Ozge Somuncu[a,b], Alexandre André B. A. da Costa[a,b], Sirisha Mukkavalli[a,b], Benjamin P. Lamarre[a,b], Huy Nguyen[a,b], Carter Grochala[b], Yuqing Jiao[a,c], Joyce Liu[c], Bose Kochupurakkal[a,c], Kalindi Parmar[a,b], Geoffrey I. Shapiro[a,c], and Alan D. D'Andrea[a,b,1]

Affiliations are included on p. 11.

Contributed by Alan D. D'Andrea; received July 11, 2024; accepted October 11, 2024; reviewed by George-Lucian Moldovan and Robert W. Sobol

Poly (ADP-ribose) glycohydrolase (PARG) is a dePARylating enzyme which promotes DNA repair by removal of poly (ADP-ribose) (PAR) from PARylated proteins. Loss or inhibition of PARG results in replication stress and sensitizes cancer cells to DNA-damaging agents. PARG inhibitors are now undergoing clinical development for patients having tumors with homologous recombination deficiency (HRD), such as cancer patients with germline or somatic *BRCA1/2*-mutations. PARP inhibitors kill BRCA-deficient cancer cells by increasing single-stranded DNA gaps (ssGAPs) during replication. Here, we report that, like PARP inhibitor (PARPi), PARG inhibitor (PARGi) treatment also causes an accumulation of ssGAPs in sensitive cells. PARGi exposure increased accumulation of S-phase-specific PAR, a marker for Okazaki fragment processing (OFP) defects on lagging strands and induced ssGAPs, in sensitive cells but not in resistant cells. PARGi also caused accumulation of PAR at the replication forks and at the ssDNA sites in sensitive cells. Additionally, PARGi exhibited monotherapy activity in specific HR-deficient, as well as HR-proficient, patient-derived, or patient-derived xenograft (PDX)-derived organoids of ovarian cancer, and drug sensitivity directly correlated with the accumulation of ssGAPs. Taken together, PARGi treatment results in toxic accumulation of PAR at replication forks resulting in ssGAPs due to OFP defects during replication. Regardless of the *BRCA*/HRD-status, the induction of ssGAPs in preclinical models of ovarian cancer cells correlates with PARGi sensitivity. Patient-derived organoids (PDOs) may be a useful model system for testing PARGi sensitivity and functional biomarkers.

PARG inhibitor | PARylation | single-stranded DNA (ssDNA) gaps | functional biomarkers | organoid models

Significance

As Poly (ADP-ribose) glycohydrolase (PARG) inhibitors are now in clinical trials, we evaluated the mechanism of replication defects resulting in tumor cell killing from PARG inhibition. We determined that PARG inhibitor treatment causes accumulation of ssGAPs in ovarian cancer preclinical models, including patient-derived organoid (PDO) models, and this phenotype directly correlates with drug sensitivity. The detection of ssGAPs in PDOs may provide a functional biomarker for predicting the response to PARG inhibitors in clinical trials.

PARylation (Poly-ADP-Ribosylation), a reversible post-translational modification of proteins, is one of the earliest waves of signaling at DNA lesions and a critical event in DNA damage response (DDR) and repair process (1, 2). Upon DNA damage, the majority of the cellular PARylation events are carried out by Poly(ADP-ribose) polymerase 1 (PARP1) using NAD+ as an ADP-ribose donor. PARP1 is rapidly recruited to single-stranded DNA (ssDNA) break sites, initiating auto-PARylation as well as modifications of histones and other proteins through mono(ADP-ribosylation) and PARylation. These modifications facilitate recruitment of various DNA repair proteins to the DNA damage sites and promote chromatin relaxation (3). Following PARylation, dePARylation is a crucial step to ensure the DDR repair factors are released from the DNA lesion for repair to occur (4, 5). Most cellular PARylation is degraded by PARG. Inefficient dePARylation results in trapping of proteins in the vicinity of the DNA lesion and impairment of DNA repair (6–8). Indeed, loss or inhibition of PARG sensitizes cancer cells to DNA-damaging agents (9, 10). Furthermore, hyperaccumulation of PAR chains can cause significant alteration in NAD+ levels, potentially hindering with NAD+-dependent processes such as ATP synthesis resulting in metabolic catastrophe (11).

Inhibition of PARP1 results in synthetic lethality in tumors with defects in homologous recombination (HR)-mediated DNA repair (12, 13). PARP inhibitors have been FDA-approved for maintenance therapies in the management of patients with high-grade serous ovarian cancer (HGSOC) in both relapsed and first-line settings (14, 15). However, de novo or acquired PARP inhibitor (PARPi) resistance is a pressing problem in the clinic and new targeted therapies are needed for the treatment of ovarian cancer patients. Recent studies have demonstrated that PARPi sensitivity stems, at least in part, from single-stranded DNA gap (ssGAP) formation and Okazaki fragment processing

Competing interest statement: A.D.D. reports consulting for AbbVie, Deerfield Management Company L.P., Impact Therapeutics, PrimeFour Therapeutics, Schrödinger Inc., and Servier Bio-Innovation LLC; is an Advisory Board member for Covant Therapeutics, and Impact Therapeutics; stockholder in Impact Therapeutics, and PrimeFour Therapeutics; and reports receiving commercial research grants from Bristol Myers Squibb, EMD Serono, Moderna, and Tango Therapeutics. G.I.S. reports grant support from Merck KGaA/EMD-Serono, Tango Therapeutics, Bristol Myers Squibb, and Merck & Co., all related to DNA repair inhibitors, as well as from Eli Lilly and Pfizer. He has served on advisory boards for Merck KGaA/EMD-Serono, Circle Pharmaceuticals, Schrödinger, Janssen and Xinthera. He holds patents entitled, "Dosage regimen for sapacitabine and selicilib," also issued to Cyclacel Pharmaceuticals, and "Compositions and methods for predicting response and resistance to CDK4/6 inhibition." J. Liu reports personal fees from AstraZeneca, Bristol Myers Squibb, Clovis Oncology, Daiichi Sankyo, Eisai, Genentech/Roche, GlaxoSmithKline, Regeneron Therapeutics, Revolution Medicine, Zentalis Pharmaceuticals, and Deciphera Pharmaceuticals outside the submitted work and institutional funding for clinical trials from 2X Oncology, Aravive, Arch Oncology, AstraZeneca, Bristol Myers Squibb, Clovis Oncology, GlaxoSmithKline, Impact Therapeutics, Pfizer, Regeneron, Seagen, SystImmune, Vigeo Therapeutics, and Zentalis Pharmaceuticals.

[1]To whom correspondence may be addressed. Email: Alan_Dandrea@dfci.harvard.edu.

This article contains supporting information online at https://www.pnas.org/lookup/suppl/doi:10.1073/pnas.2413954121/-/DCSupplemental.

Published November 15, 2024.

(OFP) deficiency during replication (16). PARP inhibitors increase ssGAPs in BRCA1-deficient cancer cells, and these ssGAPs are suppressed in resistant tumors (16, 17).

ssGAPs are the stretches of single-stranded DNA structures on the replication forks which arise during replication stress (18). These gaps build up on both the leading and lagging strand of newly synthesized DNA after treatment with many DNA-damaging agents (19–23). ssGAPs arise from OFP defects on lagging strands or from PRIMPOL-mediated repriming on leading strands in BRCA1/2-deficient cells (19, 24–27). For maintenance of genomic stability, the ssGAPs left behind advancing replication forks must be properly repaired by gap filling or post-replicative repair mechanisms, such as Translesion DNA Synthesis (TLS) repair (20, 21, 23) or by POLQ-mediated gap filling (28–30). Accordingly, TLS inhibitors and POLQ inhibitors also enhance ssGAPs in BRCA1-deficient cells (19, 20, 23, 29, 30). Recently USP1 inhibition has been shown to increase ssGAPs resulting from enhanced ubiquitination of PCNA and RAD18 trapping at the replication fork (22). Furthermore BRCA1-deficient cells are sensitive to OFP inhibition (16, 31, 32). These data suggest that ssGAPs may serve as a key determinant for various DDR inhibitor-mediated synthetic lethality.

PARG is recruited to DNA damage sites by PAR-dependent and PCNA-dependent mechanisms, suggesting that PARG has a S phase-specific function during replication (33, 34). Indeed, PARG is involved in multiple functions at the replication fork (6, 8, 35–38). During DDR, PARG promotes fork restart and cell cycle progression (6, 36). Moreover, S phase PARylation has been shown to be a sensor of defects in the OFP at the lagging strand during normal DNA replication (39). Furthermore, when OFP is inhibited by a FEN1 inhibitor, elevated levels of S phase PARylation are observed, resulting in increased sensitivity to PARP1/2 loss (39).

PARG is a potential therapeutic target for cancer therapy. Accordingly, there are two ongoing clinical trials with PARG inhibitors mainly targeting HR-deficient solid tumors (NCT05787587, NCT06395519) and biomarkers of response to these inhibitors are needed. Some reports have shown that *BRCA* and HR status predict PARGi sensitivity, whereas other reports suggest that it is not BRCAness but replication gene expression that predicts the sensitivity of PARGi (9, 36, 40). PARG inhibitors can cause excessive accumulation of PAR chains and exacerbate replication stress and DNA damage in ovarian cancer cells (9, 35, 36, 40). Specifically, PARG inhibition results in impairment of replication fork dynamics such as reduced replication fork progression, increased reversed forks, and increased fork stalling and reduced capacity of replication restart (6, 36, 38, 41). Importantly, PARG loss also causes accumulation of ssDNA, ultimately leading to replication catastrophe and DSBs (36, 41). However, the mechanism by which PARG inhibition promotes these replication errors and DNA damage in cancer cells remains elusive. The exact DNA replication vulnerability that renders ovarian cancer cells sensitive to PARGi remains unknown.

Here, we investigated the molecular mechanisms underlying PARGi sensitivity and resistance in ovarian cancer models and identified predictive biomarkers for PARGi response. We determined that PARG inhibitors promote the formation of ssGAPs in preclinical ovarian cancer models. PARGi treatment increased the levels of toxic S phase PAR resulting from OFP defects. Regardless of the *BRCA*/HRD-status, the induction of ssGAPs correlated with PARGi sensitivity in preclinical ovarian cancer models, including the patient-derived organoid (PDO) models of ovarian cancer. ssGAP accumulation in PDOs may therefore be a functional biomarker for predicting the response of ovarian cancer patients to PARG inhibitors.

Results

PARG Inhibition Causes Accumulation of Toxic S Phase PAR and Replication Stress in Sensitive Ovarian Cancer Cells. To dissect the molecular mechanism of PARGi sensitivity in ovarian cancer, we used PDD00017273 (referred to as PARGi hereafter) (36, 42) and identified sensitive and resistant ovarian cancer cell lines (*SI Appendix*, Fig. S1*A*). Consistent with the PARG dependency project Achilles (DepMap Public 22Q1) (43) data, both the RMUGS (*BRCA1/2*-wild-type) and KURAMOCHI (*BRCA2*-mutated) ovarian cancer cell lines were highly dependent on PARG for survival, compared to the OVCAR3 and COV362 (*BRCA1*-mutated) ovarian cancer cell lines (*SI Appendix*, Fig. S1 *A* and *B*). BRCA1-deficient RPE TP53$^{-/-}$ BRCA1$^{-/-}$ cells and UWB1.289 ovarian cancer cells, as well as the BRCA2-deficient DLD1 cells, were also sensitive to a PARGi (*SI Appendix*, Fig. S1*C*). Like PARG inhibition, silencing of PARG by siRNA also resulted in reduced growth of PARGi-sensitive cells but not of PARGi-resistant cells (*SI Appendix*, Fig. S1 *D* and *E*).

To determine the mechanism of sensitivity and resistance with PARGi, we next generated an isogenic cell line pair. RMUGS, the most PARGi-sensitive cell line, was exposed to a gradually increasing concentrations of PARGi until the cells grew in the presence of PARGi at a similar rate as the parental line without the drug (Fig. 1*A*). The cells with acquired resistance to PARGi, namely RMUGS-R cells, exhibited an approximately 10-fold higher IC_{50} for growth inhibition by PARGi compared to the sensitive parental cells (Fig. 1*B*). PARGi treatment resulted in similar levels of total PARylation in both sensitive and resistant cells, demonstrating similar target engagement between the sensitive and resistant cells (*SI Appendix*, Fig. S1 *F* and *G*). A high baseline level of PARP1 autoPARylation was observed in RMUGS, and this level was further increased after PARGi exposure (*SI Appendix*, Fig. S1*H*). The signal of autoPARylated PARP1 decreased after PARPi treatment, indicating that the high molecular weight protein smear above PARP1 corresponds to auto-PARylated PARP1. Interestingly, the level of auto-PARylated PARP1 was diminished in the RMUGS-R cells, suggesting reduced PARP1 activation (*SI Appendix*, Fig. S1*H*).

Unprocessed Okazaki fragments during replication can lead to genomic instability and replication defects (16, 41, 44, 45). PAR synthesis or PARP activity is detected in normal unperturbed cells during S phase due to OFP defects (39). PARGi treatment results in S-phase-specific PARylation (46). We therefore determined whether there is an S-phase-specific difference in PARylation levels between the sensitive and resistant cells. PARGi increased the level of S-phase-specific PAR more significantly in RMUGS than in RMUGS-R cells (Fig. 1*C*). PARGi-induced S phase PAR levels were significantly higher in the PARGi-sensitive RPE TP53$^{-/-}$ BRCA1$^{-/-}$ cells compared to RPE TP53$^{-/-}$ cells (Fig. 1*D*). These results were also confirmed in ovarian cancer cell lines with de novo sensitivity or resistance in the presence of PARGi or PARG knockdown with siRNA (*SI Appendix*, Fig. S1 *I–L*).

Toxic accumulation of S phase PAR after PARG inhibition can lead to replication defects. We therefore assessed DNA damage and replication stress in PARGi-sensitive and resistant models. Consistent with previous findings (36) inhibition or knock-down of PARG led to elevated replication stress and DNA damage markers, including increased levels of p-CHK1, p-RPA, p-KAP1, and γH2AX, in the sensitive ovarian cancer cells. However, this effect was not observed in cells with de novo or acquired resistance to

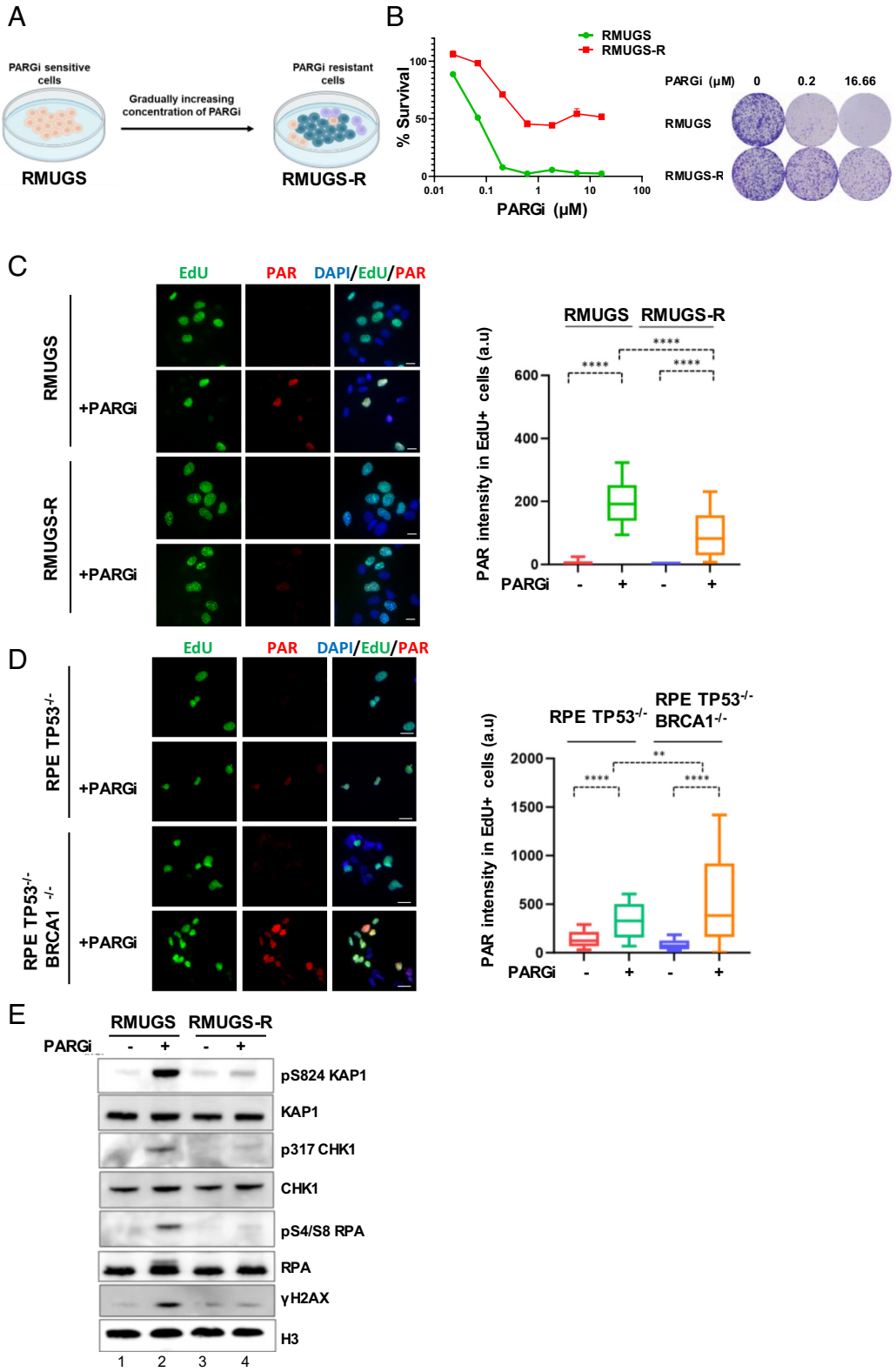

Fig. 1. PARG inhibition leads to toxic S phase PAR accumulation in sensitive cells. (*A*) Schematic of the method for generating ovarian cancer cells with acquired resistance to PARGi (PDD00017273). PARGi-sensitive cell line, RMUGS was exposed to increasing dose of PARGi over 4 mo and resistant cells were derived (RMUGS-R). (*B*) Clonogenic survival of RMUGS and RMUGS-R cells in the presence of increasing concentration of PARGi. *Left*: Graphical quantitation of the colonies from cells treated with PARGi compared to control cells treated with DMSO (IC50 RMUGS—0.07 μM and RMUGS-R—0.61 μM). *Right*: Representative images of the colonies. (*C*) *Left*: Representative images of EdU and PAR staining showing S phase PARylation after DMSO or PARGi (10 μM) treatment for 2 h in RMUGS and RMUGS-R cells. Scale 10 μm. *Right*: Quantification of S phase PARylation in RMUGS and RMUGS-R cells. Whiskers represent the minimum and maximum (****$P < 0.0001$; Mann–Whitney test). (*D*) *Left*: Representative images of EdU and PAR staining showing S phase PARylation after DMSO or PARGi (10 μM) treatment for 2 h in RPE TP53$^{-/-}$ and RPE TP53$^{-/-}$ BRCA1$^{-/-}$ cells. Scale 10 μm. *Right*: Quantification of S phase PARylation in RPE TP53$^{-/-}$ and RPE TP53$^{-/-}$ BRCA1$^{-/-}$ cells. Whiskers represent the minimum and maximum (****$P < 0.0001$; **$P = 0.0044$; Mann–Whitney test). (*E*) Western blot showing replication stress and DNA damage markers after PARGi treatment (10 μM) in RMUGS and RMUGS-R cells.

PARGi (Fig. 1*E* and *SI Appendix*, Fig. S1 *M* and *N*). Additionally, RNA sequencing analysis performed with RMUGS and RMUGS-R cells revealed upregulation of DNA replication gene expression in the PARGi resistant RMUGS-R cells, accounting, at least in part, for the reduced replication stress (*SI Appendix*, Fig. S1*O*).

Collectively, these results demonstrate that PARGi-sensitive ovarian cancer cells, but not drug-resistant cells, exhibit higher levels of S-phase-specific PAR and replication stress, accounting at least in part for the cell death upon PARG inhibition.

PARG Inhibition or PARG Loss Leads to Increased ssGAP Formation in Sensitive Cells. Recent studies have identified ssGAPs as a key determinant of the sensitivity of BRCA1-deficient cells to PARP inhibition (16), or to other DNA repair inhibitors (22, 30). BRCA1-deficient cells have an increased basal level of S phase PAR, due to OFP defects, which ultimately leads to the formation of ssGAPs on lagging strands (16). Since PARGi exposure also increases S phase PAR and replication stress in sensitive cells, we hypothesized that the cytotoxicity of the drug might result from the enhancement of ssGAPs originating from OFP defects on lagging strands.

We therefore employed DNA fiber assays, followed by S1 nuclease treatment, to detect ssGAPs (47). Interestingly, PARG inhibition increased the number of ssGAPs in RMUGS cells; however, the gaps were suppressed in RMUGS-R cells (Fig. 2 *A* and *B* and *SI Appendix*, Fig. S2*A*). As expected, PARPi increased ssGAPs in RPE TP53$^{-/-}$ BRCA1$^{-/-}$ cells. PARG inhibition also increased ssGAPs in PARGi-sensitive BRCA1-deficient cells but not in PARGi resistant parental RPE TP53$^{-/-}$ cells (Fig. 2 *C* and *D*). Similarly, PARGi exposure resulted in ssGAP accumulation in KURAMOCHI cells, but not in COV362 cells, correlating with their relative drug sensitivity versus resistance (*SI Appendix*, Fig. S2 *B* and *C*). These results suggested that, regardless of the *BRCA*/HRD status, the induction of ssGAPs in ovarian cancer cells correlates with PARGi sensitivity.

To confirm that PARG suppresses ssGAPs, we generated a CRISPR knockout of PARG in RPE TP53$^{-/-}$ cells. These RPE TP53$^{-/-}$ PARG$^{-/-}$ cells did not accumulate ssGAPs. Following a BRCA1 depletion, there was a significant increase in the accumulation of ssGAPs in RPE TP53$^{-/-}$ PARG$^{-/-}$ cells, while this accumulation was not observed in the parental RPE TP53$^{-/-}$ cells (Fig. 2 *E* and *F* and *SI Appendix*, Fig. S2 *D* and *E*). To investigate whether ssGAP suppression is associated with the catalytic activity of PARG, we reconstituted RPE TP53$^{-/-}$ PARG$^{-/-}$ cells with the cDNA encoding either the wildtype PARG enzyme (PARG-WT) or a catalytically inactive mutant (PARG-MUT). Complementation with PARG-WT not only reduced PARylation but also suppressed the ssGAPs in RPE TP53$^{-/-}$ PARG$^{-/-}$ cells with BRCA1 knockdown (Fig. 2 *G* and *H* and *SI Appendix*, Fig. S2 *F* and *G*). In contrast, the expression of the PARG-MUT failed to suppress ssGAPs and failed to reduce PAR levels (Fig. 2 *G* and *H* and *SI Appendix*, Fig. S2 *F* and *G*). Consistent with this increase in ssGAP accumulation, BRCA1 depletion reduced the survival of RPE TP53$^{-/-}$ PARG$^{-/-}$ cells but not of the RPE TP53$^{-/-}$ cells (*SI Appendix*, Fig. S2*H*).

Collectively these data indicate that PARG inhibition or PARG loss causes an increase in ssGAPs in drug-sensitive cells but not in drug-resistant cells. Moreover, the catalytic activity of PARG is required for suppressing ssGAP accumulation.

PARG Inhibition Increases the Level of PARylated Proteins at ssDNA in Sensitive Cells. In sensitive cells, PARG inhibition causes elevated S phase PAR and the accumulation of ssGAPs (Fig. 1 *C* and *D* and 2 *B* and *D* and *SI Appendix*, Fig. S1 *I* and *J* and S2 *A* and *B*). We therefore reasoned that an accumulation of PARylated proteins at the replication fork would correlate with an increase in ssGAPs and DNA damage. To test this hypothesis, we conducted a quantitative in situ analysis of protein interactions at DNA replication forks (SIRF) assay (48). This assay employs proximity ligation chemistry to identify protein interactions with nascent DNA replication forks. In RMUGS cells, but not in RMUGS-R cells, PAR was associated with nascent DNA replication forks in the untreated condition, and increased PAR was observed after PARGi treatment (Fig. 3*A*). The accumulation of PAR at the nascent DNA replication sites after exposure to PARGi was also confirmed in RPE BRCA1 deficient cells and PARG$^{-/-}$ cells after BRCA1 knockdown (*SI Appendix*, Fig. S3 *A* and *B*). Consistent with the accumulation of ssGAPs in sensitive cells after PARGi exposure, there was an increase in pRPA, a ssDNA surrogate replication stress marker, at replication forks after PARG inhibition in RMUGS cells (*SI Appendix*, Fig. S3*C*). p-RPA sites also colocalized with PAR, and this colocalization was significantly increased after PARGi treatment in RMUGS cells and in PARG$^{-/-}$ cells after BRCA1 knockdown (Fig. 3*B* and *SI Appendix*, Fig. S3*D*). These results suggest that the accumulation of PAR occurs at ssDNA sites after PARG inhibition in sensitive cells.

Next, we identified proteins that are recruited to nascent replication forks after PARG inhibition by using a combination of the aniPOND assay and Mass spectrometry (MS) (49). Multiple DNA repair proteins, including XRCC1, PNKP, CHD1L, and PARP14, were enriched at replication forks after PARGi treatment in RMUGS cells (Fig. 3*C*). Interestingly, some of these proteins are known to be PARylated or recruited via PARylation (50). Furthermore, proteins involved in the BER or OFP pathways (e.g., XRCC1, PNKP, LIG3, IMPDH2) and the NAD/metabolic pathway (e.g., GLUD1/2) were specifically enriched (51). XRCC1, a scaffold protein, binds and recruits proteins involved in single strand break repair at the forks (52, 53). With the aniPOND assay, followed by western blot, we confirmed the enrichment of PAR and XRCC1 at replication forks after PARG inhibition (Fig. 3*D*). The accumulation of XRCC1 at the nascent replication forks in RMUGS cells was further validated (Fig. 3*E*). PARGi treatment also increased the recruitment of XRCC1 to nascent replication forks in RPE BRCA1 deficient cells (*SI Appendix*, Fig. S3*E*). Interestingly, this increase in XRCC1 at nascent replication forks was not observed in RMUGS-R-resistant cells (Fig. 3*E*). MRE11, a nuclease involved in DSB repair, was also detected at replication forks and further enriched after PARG inhibition (Fig. 3*D*). PARP14 has been shown to bind nascent DNA and promote MRE11 recruitment to DNA (54). Both PARP14 and MRE11 were recruited at the replication forks in PARG-inhibited cells (Fig. 3 *C* and *D*), suggesting that these proteins may be recruited as a complex. Since MRE11 is known to expand ssGAPs (55, 56) we determined whether its recruitment promotes PARGi-induced ssGAP accumulation. MRE11 knockdown in PARGi-sensitive cells did not alter the ssGAP accumulation or drug sensitivity after PARGi treatment (*SI Appendix*, Fig. S3 *F, G,* and *H*), suggesting that PARGi-induced ssGAPs and cell death are not dependent on MRE11.

Taken together, the persistent PARylation of proteins, the accumulation of ssGAPs, and the toxic accumulation of XRCC1 at the replication fork may account, at least in part, for the enhanced cytotoxicity of PARGi in the sensitive cells.

PARG Inhibition Causes Increased PARylation at the Okazaki Fragments. We next evaluated the mechanism of ssGAP accumulation after PARG inhibition. Since PARGi-sensitive cells

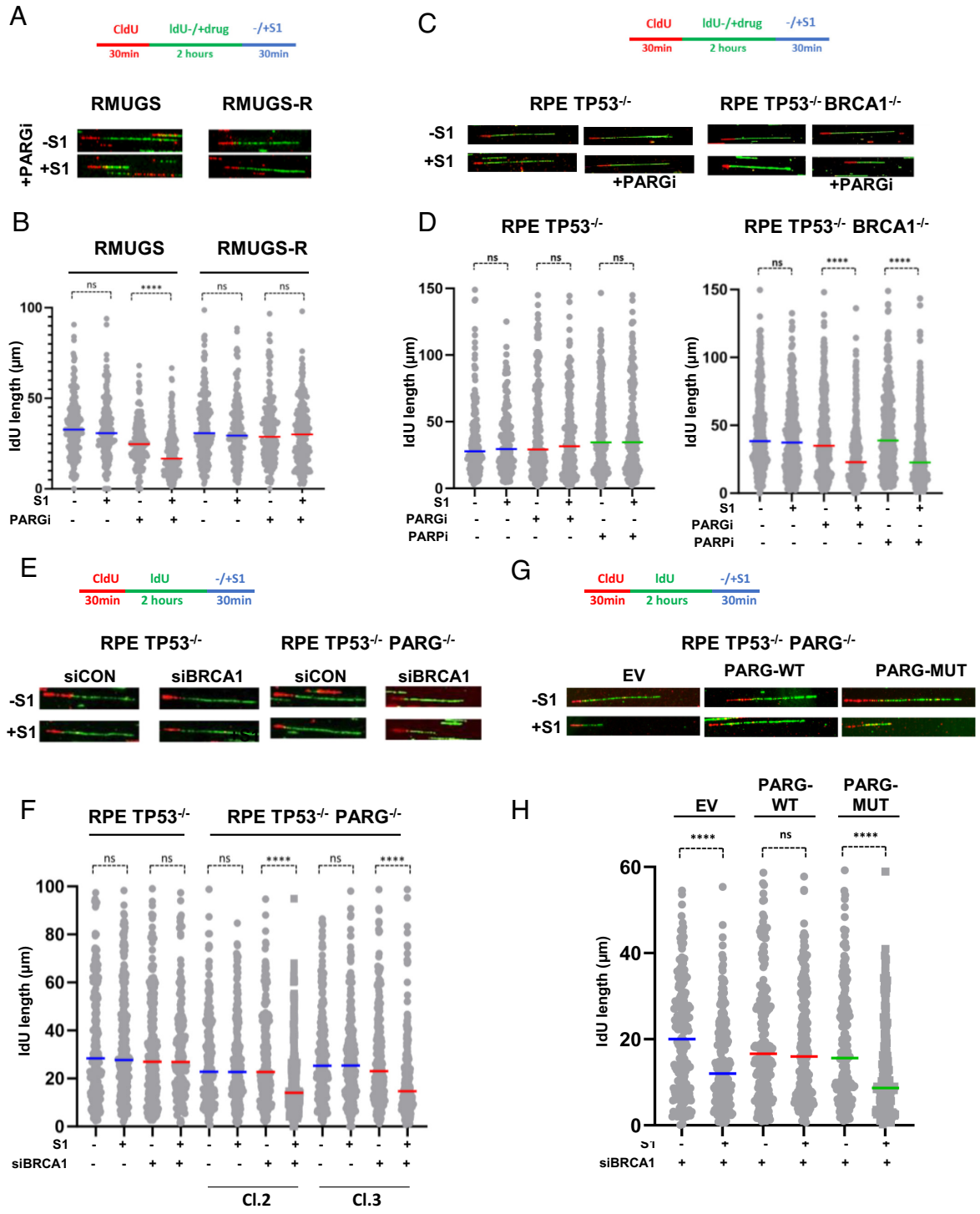

Fig. 2. PARG inhibition or PARG loss results in accumulation of ssGAPs in drug-sensitive but not drug-resistant cells. (*A*) *Top*: Schematic of DNA fiber assay with CldU/IdU pulse-labeling protocol and drug treatment, followed by S1 nuclease treatment. *Bottom*: Representative DNA fiber images in RMUGS and RMUGS-R cells after PARG inhibition with or without S1 nuclease treatment. (*B*) Quantification of IdU tracts from RMUGS and RMUGS-R cells after PARGi (10 µM) treatment with or without S1 nuclease. Each dot represents one fiber. At least 200 fibers were analyzed per condition. Median values are represented by horizontal lines (n.s., not significant; ****$P < 0.0001$; Mann–Whitney test). (*C*) *Top*: Schematic of DNA fiber assay with CldU/IdU pulse-labeling protocol and drug treatment, followed by S1 nuclease treatment. *Bottom*: Representative DNA fiber images in RPE TP53$^{-/-}$ and RPE TP53$^{-/-}$ BRCA1$^{-/-}$ cells after PARG inhibition with or without S1 nuclease treatment. (*D*) Quantification of IdU tracts from RPE TP53$^{-/-}$ and RPE TP53$^{-/-}$ BRCA1$^{-/-}$ cells after PARGi (10 µM) treatment. Each dot represents one fiber. At least 200 fibers were analyzed per condition. Median values are represented by horizontal lines (n.s., not significant; ****$P < 0.0001$; Mann–Whitney test). (*E*) *Top*: Schematic of DNA fiber assay with CldU/IdU pulse-labeling protocol followed by S1 nuclease treatment. *Bottom*: Representative DNA fiber images in RPE TP53$^{-/-}$ and RPE TP53$^{-/-}$ PARG$^{-/-}$ cells after BRCA1 knockdown with or without S1 nuclease treatment. (*F*) Quantification of IdU tracts in RPE TP53$^{-/-}$ and RPE TP53$^{-/-}$ PARG$^{-/-}$ cells after BRCA1 knockdown with or without S1 nuclease. Each dot represents one fiber. At least 200 fibers were analyzed per condition. Median values are represented by horizontal lines (n.s., not significant; ****$P < 0.0001$; Mann–Whitney test). (*G*) *Top*: Schematic of DNA fiber assay with CldU/IdU pulse-labeling protocol followed by S1 nuclease treatment. *Bottom*: Representative DNA fiber images in RPE TP53$^{-/-}$ PARG$^{-/-}$ cells after transfection with siBRCA1 and cDNA encoding Empty vector (EV), PARG wildtype (PARG-WT), or catalytically dead PARG mutant (PARG-MUT) with or without S1 nuclease treatment. (*H*) Quantification of IdU tracts from RPE TP53$^{-/-}$ PARG$^{-/-}$ cells after transfection with siBRCA1 and EV, PARG-WT, or PARG-MUT with or without S1 nuclease. Each dot represents one fiber. At least 200 fibers were analyzed per condition. Median values are represented by horizontal lines (n.s., not significant; ****$P <$ 0.0001; Mann–Whitney test).

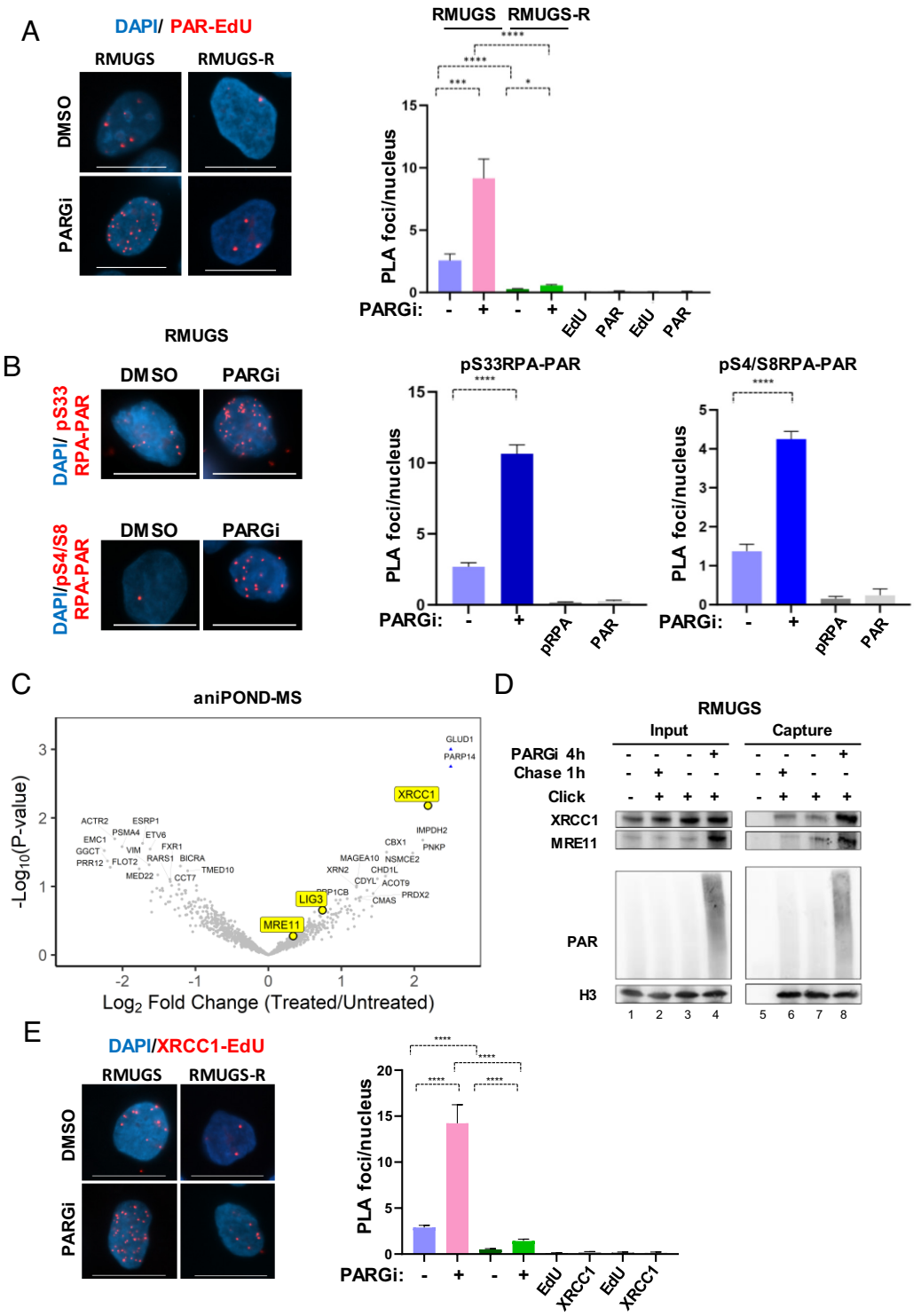

Fig. 3. PARG inhibition leads to accumulation of PAR at the ssDNA sites of replication forks in sensitive cells. (*A*) *Left*: Representative image of SIRF assay performed to detect PAR-EdU proximity ligation assay (PLA) foci at the replication forks after PARG inhibition in RMUGS and RMUGS-R cells. Scale 10 μm. *Right*: Quantification of PAR-EdU PLA foci at the replication forks after PARG inhibition (10 μM) for 2 h in RMUGS and RMUGS-R cells. PLA performed with either anti-Biotin (EdU) or anti-PAR antibody alone as negative controls are also shown. Mean and SEM values are represented (****$P < 0.0001$; ***$P < 0.001$; *$P = 0.0189$; Mann–Whitney test). (*B*) *Left*: Representative image of PAR-pRPA (pS33 RPA and pS4/S8 RPA) PLA foci after PARG inhibition in RMUGS cells. Scale 10 μm. *Right*: Quantification of PAR-pRPA PLA foci after PARG inhibition (10 μM) for 2 h in RMUGS cells. PLA performed with either anti-pRPA or anti-PAR antibody alone as negative controls are also shown. Mean and SEM values are represented (****$P < 0.0001$; Mann–Whitney test). (*C*) Volcano plot from aniPOND assay coupled with mass spectrometry (MS) showing enrichment of proteins at the replication forks after PARGi exposure in RMUGS cells. Samples treated with PARGi (10 μM) for 4 h were compared to the samples treated with DMSO. (*D*) Western blot from aniPOND assay showing enrichment of PAR, XRCC1, and MRE11 at replication forks after treatment with PARGi. (*E*) *Left*: Representative image of XRCC1-EdU PLA foci at the replication fork after PARG inhibition in RMUGS and RMUGS-R cells. Scale 10 μm. *Right*: Quantification of XRCC1-EdU PLA foci at the replication fork after PARG inhibition (10 μM) for 2 h in RMUGS and RMUGS-R cells. PLA performed with either anti-Biotin (EdU) or anti-XRCC1 antibody alone as negative controls are also shown. Mean and SEM values are represented (****$P < 0.0001$; Mann–Whitney test).

have increased S phase PARylation, we hypothesized that these cells have increased unligated Okazaki fragments or OFP defects on the lagging strand. To test this hypothesis, the level of S phase PARylation in RMUGS cells was measured after incubation with emetine (EME), an inhibitor of DNA replication that prevents the formation of Okazaki fragments, thereby uncoupling leading and lagging strand DNA replication (57). Although a recent study suggests that EME is not a specific inhibitor of Okazaki fragment formation (58), it has been used previously to study PARylation resulting from the defects in Okazaki fragment formation (39, 46). We also used a FEN1 inhibitor (FEN1i) which perturbs OFP (39). As expected, PARG inhibition increased S phase PARylation; however, a combination of EME plus PARG inhibition significantly reduced S phase PAR levels, suggesting that EME treatment prevents PARP activation at sites of unligated Okazaki fragments in RMUGS cells (Fig. 4*A*). On the other hand, treatment with FEN1i in combination with PARGi significantly increased S phase PAR due to increased Okazaki processing defects (Fig. 4*A*).

We next analyzed the level of PAR at the nascent replication forks after treatment with EME or FEN1i in the presence of PARGi. Similar to the S Phase PAR results, EME substantially decreased PAR levels at replication forks while FEN1 inhibition increased PAR levels at nascent replication forks post PARG inhibition (Fig. 4*B*). Furthermore, PAR colocalization with pRPA sites increased after FEN1 inhibition (Fig. 4*C*).

ssGAPs can also result from PRIMPOL-mediated repriming on both the leading and lagging strands of a replication fork (19, 25, 59, 60). To determine whether the accumulation of ssGAPs occurs mainly on lagging strands, due to OFP defects, we performed DNA fiber assay with S1 nuclease in PARGi-sensitive cells after PRIMPOL depletion. Interestingly, knockdown of PRIMPOL did not alter the drug sensitivity or ssGAP accumulation after PARG inhibition of PARGi-sensitive cells (*SI Appendix*, Fig. S4 *A*–*F*).

Collectively, these results suggest that majority of the PARylation at replication forks resulting from PARG inhibition occurs in the close proximity to unligated Okazaki fragments. Excessive PARylation appears to impede the OFP, resulting in an accumulation of ssGAPs and eventual cell killing (Fig. 4*D*).

PARGi Sensitivity Correlates with ssGAP Accumulation in Ovarian Cancer PDOs. PDOs provide a useful model system for rapid functional testing and prediction of drug sensitivity (61–63). Organoid models are excellent preclinical models due to their ability to recapitulate the true characteristics of a tumor from which they were derived. Ovarian tumor organoids also grow quickly, and little genetic drift occurs in this short time frame (61).

PDOs were generated from fresh tumor resections, ascites, or pleural effusion samples derived from ovarian cancer patients (*SI Appendix*, Table S7). Among the five PDOs, two were from patients with germline *BRCA1* mutation (DF3602 and DF3888). One of the models (DF4195), was *BRCA1/2*-wild-type but the patient's tumor was HRD+ according to the Myriad myChoice assay (64). The remaining two PDOs were *BRCA1/2*-wild-type. Organoids from *BRCA1*-mutated patients (DF3602 and DF3888) displayed morphologic and histological features of HGSOC (Fig. 5*A*). These organoids stained positive for the PAX8, WT1, and mutant p53, the hallmark markers of ovarian cancer tumors (Fig. 5*B*). Interestingly, DF3602 was sensitive to both PARPi and PARGi, however, DF3888 was sensitive to PARPi but not to PARGi (Fig. 5*C* and *SI Appendix*, Fig. S6*A*). The *BRCA1/2*-wildtype PDO (DF4649) was sensitive to both PARPi and PARGi. However, another model DF4195 which is *BRCA1/2* wildtype HRD+ was PARPi-sensitive but PARGi-resistant. The *BRCA1/2* wildtype model (DF4733) was resistant to both PARPi and PARGi (Fig. 5*C* and *SI Appendix*, Fig. S6*A*).

We also assessed the drug sensitivity of organoids derived from PARPi sensitive or resistant PDX-derived organoids (PDXOs) of HGSOC (65) (*SI Appendix*, Fig. S5 *A* and *B*). Interestingly, PARGi exhibited monotherapy activity in a specific HR-deficient PARPi-sensitive PDXO model DF83 with *RAD51C* hypermethylation and in a HR-proficient PDXO model DF106. However, the *BRCA1*-mutated PARPi resistant PDXO models (DF59, DF86, and DF101) were resistant to PARGi (*SI Appendix*, Fig. S5*C* and S6*B*). These results demonstrate that PARGi sensitivity is distinct from PARPi sensitivity and that PARGi are even effective in some HR-proficient organoid models of ovarian cancer.

In ovarian cancer cell lines, PARGi induced the accumulation of ssGAPs in drug-sensitive cells but not in drug-resistant cells. Importantly, PARGi also induced ssGAPs in primary tumor cells derived from patients whose cells were sensitive to PARGi. Specifically, PARGi induced ssGAPs in the PARGi-sensitive DF3602 PDO model but not in the PARGi-resistant DF3888 PDO model (Fig. 5 *D*–*F*). Similarly, PARGi increased ssGAPs in a sensitive DF83 PDXO model but not in the drug-resistant DF59 or DF101 PDXO models (*SI Appendix*, Fig. S5 *D*–*F*). These data are summarized in *SI Appendix*, Fig. S6 *C* and *D*.

Collectively, PARGi exposure resulted in the accumulation of ssGAPs in PDOs or PDXOs of ovarian cancer and this phenotype directly correlated with drug sensitivity.

Inhibitors of ATR/CHK1/WEE1 Axis can Overcome PARGi Resistance. Replication stress can trigger cell cycle checkpoints via the ATR/CHK1 signaling pathway. Depletion of PARG or PARGi activates the ATR/CHK1 pathway and combining PARGi with CHK1 or WEE1 inhibitor enhances killing of ovarian cancer cells (6, 36, 66, 67). ATR inhibition also causes accumulation of ssGAPs by fork uncoupling, thus providing an entry point for nucleases to degrade nascent DNA structures (68). We therefore reasoned that the inhibitors of the ATR/CHK1 pathway might resensitize the PARGi-resistant ovarian cancer cells (RMUGS-R) by inducing replication stress. As predicted, the combination of a PARGi with either an ATR inhibitor (ATRi), a CHK1 inhibitor, or a WEE1 inhibitor resulted in synergistic cytotoxicity in RMUGS-R compared to the RMUGS cells (*SI Appendix*, Fig. S7 *A*–*C*). The combination of PARGi and ATRi also enhanced the drug sensitivity of PDO models (*SI Appendix*, Fig. S7*D*).

Taken together, these results provide a rationale for using a combination of PARGi with inhibitors of the ATR/CHK1/WEE1 axis for enhancing the cytotoxicity in ovarian cancer models and for overcoming drug resistance.

Discussion

Protein PARylation and dePARylation processes are vital for preserving genome stability and DNA damage response. Accordingly, both protein modification processes have been therapeutically targeted. PARP inhibitors are used in the clinic for the treatment of ovarian cancers (15, 69–71). To identify the biomarkers of response to the PARG inhibitors, we dissected the mechanism by which these agents kill ovarian cancer cells. PARGi increased toxic S-phase PARylation resulting from elevated unligated Okazaki fragments. An accumulation of PARylated proteins at replication forks was observed in sensitive but not in resistant ovarian cancer cells. A recent study also showed that PARGi cytotoxicity occurs due to excessive S-phase PAR resulting from unligated Okazaki fragments (46). Importantly, we found that PARG inhibition or

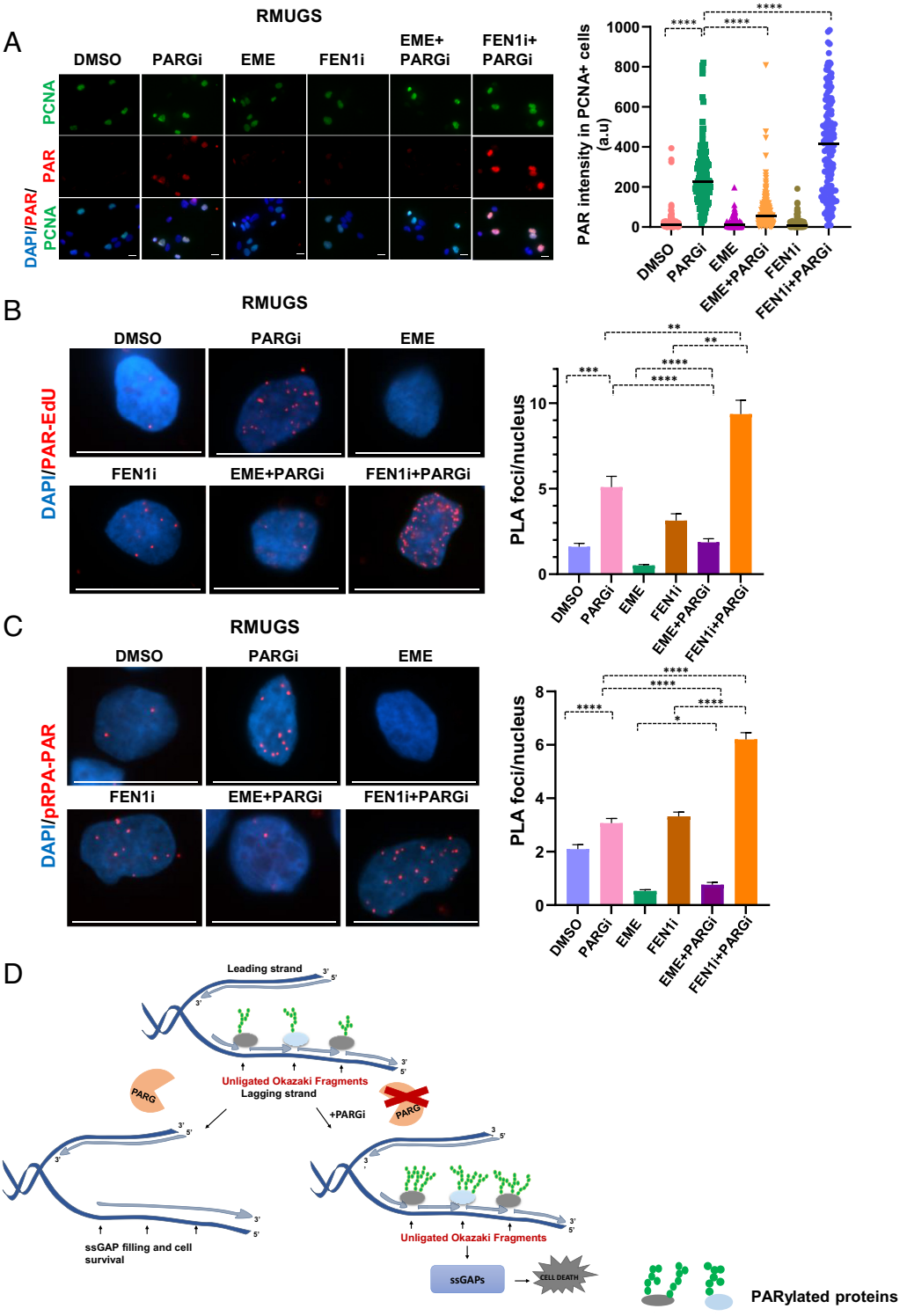

Fig. 4. Increased accumulation of PAR and ssDNA occur at unligated Okazaki fragments after PARG inhibition. (*A*) *Left*: Representative images of PCNA and PAR staining showing S phase PARylation in the presence of indicated drugs in RMUGS cells. Scale 10 μm. *Right*: Quantification of S phase PARylation in the presence of indicated drugs in RMUGS cells. Median values are represented (****$P < 0.0001$; Mann–Whitney test). (*B*) *Left*: Representative image of PAR-EdU PLA foci at the replication fork in the presence of indicated drugs in RMUGS cells. Scale 10 μm. *Right*: Quantification of PAR-EdU PLA foci at the replication fork in the presence of indicated drugs in RMUGS cells. Mean and SEM values are represented (****$P < 0.0001$; ***$P < 0.001$; **$P < 0.05$; Mann–Whitney test). (*C*) *Left*: Representative images of PAR-pRPA PLA foci in the presence of indicated drugs in RMUGS cells. Scale 10 μm. *Right*: Quantification of PAR-pRPA PLA foci in the presence of indicated drugs in RMUGS cells. Mean and SEM values are represented (****$P < 0.0001$; *$P = 0.018$; Mann–Whitney test). (*D*) Model depicting increased unligated Okazaki fragments and ssGAP accumulation after PARGi treatment in PARGi-sensitive cells.

PARG knockout results in accumulation of ssGAPs. The cellular sensitivity to PARGi correlated with the formation of ssGAPs in preclinical ovarian cancer models, thereby providing a predictive biomarker for sensitivity to this treatment. We demonstrate that this functional biomarker can predict the PARGi response of ovarian cancer models, regardless of their *BRCA*/HRD status.

Our study demonstrates that PARG activity is required to suppress ssGAPs in HR-deficient as well as in specific HR-proficient

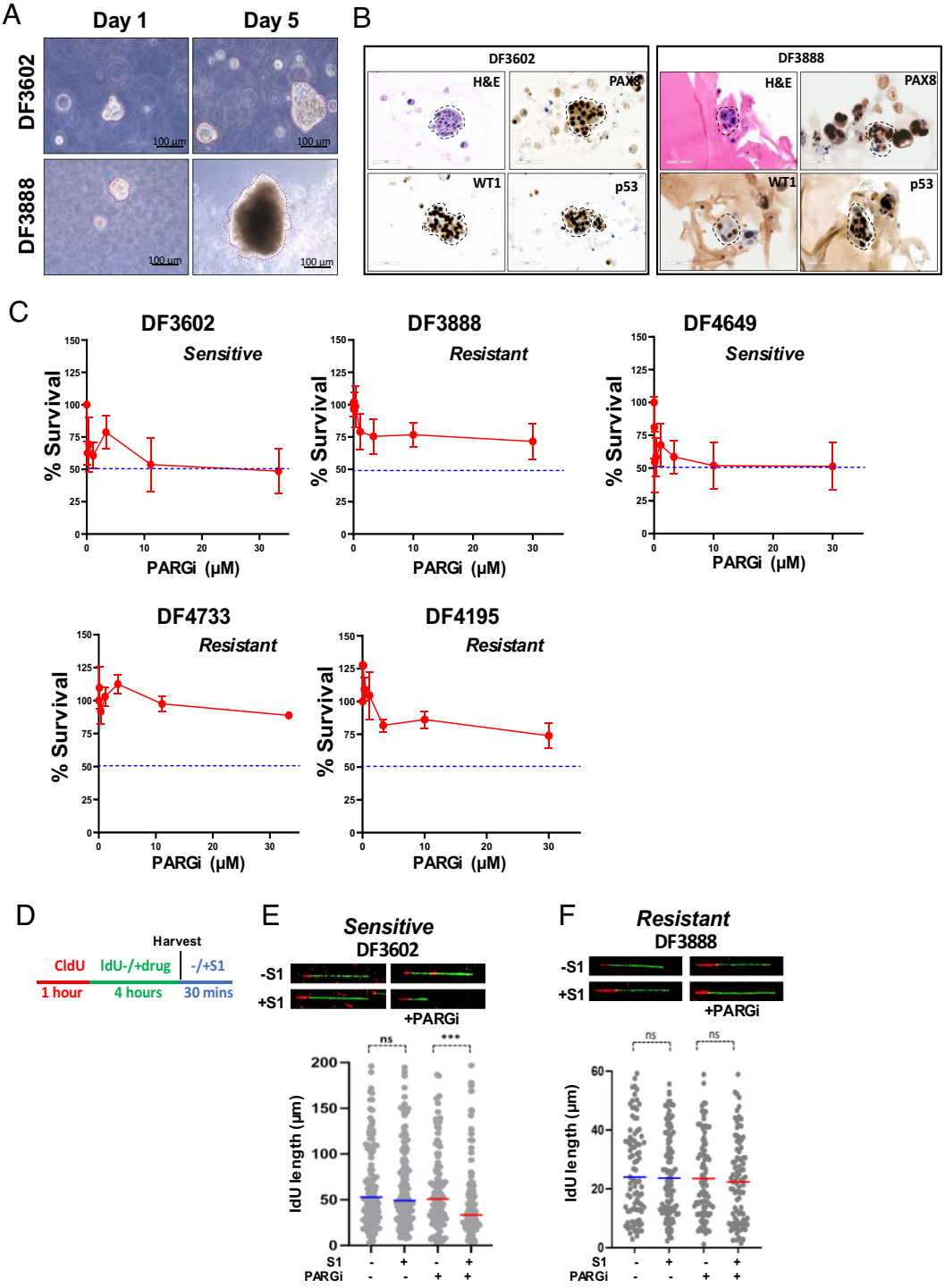

Fig. 5. PARGi sensitivity correlates with ssGAP accumulation in ovarian cancer patient-derived organoids (PDOs). (*A*) Representative images of the morphology of ovarian cancer PDOs. (*B*) Representative images of H&E and immuno-histochemistry staining of PDOs. (*C*) Survival plots of PDOs exposed to increasing concentration of PARGi. (*D*) Schematic of DNA fiber assay with CldU/IdU pulse-labeling protocol and drug treatment, followed by S1 nuclease treatment. (*E* and *F*) *Top*: Representative DNA fiber images in PDOs after PARG inhibition with or without S1 nuclease treatment. *Bottom*: Quantification of IdU tracts from PDOs after PARGi (100 µM) treatment with or without S1 nuclease. Each dot represents one fiber. At least 90 fibers were analyzed per condition. Median values are represented by horizontal lines (n.s., not significant; ***$P < 0.001$; Mann–Whitney test).

ovarian cancer cells that have inherent lagging strand defects. It remains unclear whether the drug-induced cytotoxicity arises from ssGAPs themselves, from their conversion into DSBs during replication, or from their collision with incoming replication forks.

During replication, discontinuous lagging strand synthesis generates ssGAPs between the Okazaki fragments (27). Accordingly, unligated Okazaki fragments are a source of ssGAPs (19, 27). Unligated Okazaki fragments that escape canonical processing by FEN1 and LIG1 are detected by PARylation specifically during S phase (39). PARylation by PARP1 further recruits XRCC1, a scaffold protein which interacts with LIG3 and DNA polymerase β (POLβ), leading to the processing of unligated Okazaki fragments and repair of the ssGAPs. This backup mechanism of OFP is important for completion of lagging strand synthesis in unperturbed cells. Notably, BRCA1-deficient cells have elevated S phase PARylation and defective recruitment of backup OFP pathway

(16). PARPi kills BRCA1 deficient cells, at least in part, by further increasing ssGAPs. These cells have reduced efficiency of the XRCC1-LIG3-dependent backup pathway of OFP (16). Similarly, POLQ inhibitors increase ssGAPs by interfering with the refilling of inter-Okazaki fragment gaps (72).

Ovarian cancer cells which are sensitive to PARG inhibition exhibit inherent defects in lagging strand replication and have excessive unligated Okazaki fragments. These cells require PARG activity to eliminate toxic PAR chains that build up near the Okazaki fragments and to prevent accumulation of ssGAPs. The reduction in PAR leads to more efficient refilling of these ssGAPs. Consistent with our observations, recent studies have identified synthetic lethality between components of OFP and PARG inhibition (41, 46). Consequently, cells sensitive to PARGi are reliant not only on PARG but also on factors related to OFP. Distinct from PARP inhibitors, where the ssGAPs may also arise from PRIMPOL-mediated repriming, the majority of ssGAPs caused by PARG inhibitors result from defects in OFP on the lagging strand.

By AniPOND/Mass spectrometry analysis, we demonstrated that PARGi increases the recruitment of various PARylated or PAR interacting DNA repair proteins at replication forks. For example, XRCC1, PNKP, and CHD1L (ALC1) are components of the Single-Stranded Break Repair (SSBR) and Base Excision Repair (BER) pathways and have been identified as PAR modulators (50). PAR accumulation appears to be regulated by replication-associated BER as previously described (53).

In PARGi-sensitive cell lines, XRCC1, a PAR interacting protein was among the most enriched proteins at replication forks after PARGi exposure. Our results suggest that XRCC1 is trapped at replication forks and its presence may prevent the otherwise efficient refill of the ssGAPs. The persistence of these XRCC1 lesions may hinder the recruitment of polymerases (e.g., POLβ) and the downstream ligation of Okazaki fragments. Excessive loading of XRCC1 or other PARylated proteins may interfere with canonical or backup pathways of OFP leading to the accumulation of ssGAPs after PARG inhibition in sensitive cells. These ssGAPs can lead to cell death either directly or following their conversion into DSBs by nucleases or DNA replication fork collapse. (Fig. 4*D*). Prolonged exposure of PARylated proteins can also reduce the free pool of PAR moieties, ultimately depleting cellular NAD+ levels. Such depletion has wide-ranging implications for cellular function (46, 53). Interestingly increasing NAD+ bioavailability can also enhance PARGi cytotoxicity due to hyperaccumulation of PAR chains (53).

Inhibition or depletion of PARG can also cause an elevation of reversed forks (6). Processing these reversed forks can impede replication fork progression and increase unanticipated recruitment of DNA repair factors, leading to the formation of aberrant DNA structures. Subsequently these abnormalities at DNA replication forks may disrupt DNA replication, activate cell cycle checkpoint, and contribute to genome instability (6, 73). Our data show that PARGi-sensitive cells have increased replications stress, increased DNA damage, and activation of cell cycle checkpoints. Compromised replication, as evidenced by decreased transcription of genes controlling DNA replication, is associated with sensitivity to PARGi (40). Consistent with this study, our RNA sequencing data revealed increased expression of DNA replication genes in PARGi resistant (RMUGS-R) cells compared to PARGi-sensitive (RMUGS) cells. Ovarian cancer cells with acquired resistance may have therefore adapted to high doses of PARGi by selection and increased expression of DNA replication gene products. Furthermore, we also show that combining DDR inhibitors that induce replication stress can effectively overcome acquired resistance to PARGi in these ovarian cancer cells.

Last, our findings have clinical implications. Ovarian cancer PDOs provide a model system for rapid functional testing of anticancer drugs and for predicting their therapeutic activity (63). Drug sensitivity of HGSOC organoids often correlates with the clinical responses in patients (61). HGSOC organoids, which grow rapidly in only 7 to 10 d, provide a practical tool for predicting clinical responses of individual patients and for guiding clinical decisions. In our study, we have evaluated tumor organoids derived from ovarian cancer patients who were undergoing chemotherapy such as carboplatin and paclitaxel. Additionally, we investigated the efficacy of PARGi in ovarian cancer PDXOs where we have a comprehensive mutational profiling done. Specific organoid models were responsive to PARGi regardless of the *BRCA*/HRD status. Organoids responsive to the PARGi also exhibited an accumulation of ssGAPs, further validating ssGAP generation as a functional biomarker for measuring the PARGi response.

Materials and Methods

Drugs. Following drugs were purchased from SelleckChem: PDD00017273 (Cat# S8862), Olaparib (Cat# S1060), M1774 (Cat# E1411), AZD1775 (Cat# S1525), and Prexasertib (Cat# S7178).

Cell Culture. COV362, COV318, ES2, JHOS4, KURAMOCHI, OV90, PA1, OVCAR3, OVSAHO, RMUGS, RMUGS-R, DLD1, and DLD1-BRCA2$^{-/-}$ cell lines were grown in RPMI 1640 supplemented with 10% fetal bovine serum and 1% penicillin-streptomycin (100U/mL). UWB1.289 and UWB1.289 + BRCA1 cells were grown in 50% RPMI 1640 and 50% MEBM (Lonza) supplemented with MEGM singlequots supplements (Lonza) containing bovine pituitary extract, human epidermal growth factor, insulin, hydrocortisone, gentamicin sulfate-amphotericin, 3% FBS, and 1% penicillin–streptomycin (100 U/mL). RPE TP53$^{-/-}$, RPE TP53$^{-/-}$BRCA1$^{-/-}$, RPE TP53$^{-/-}$ PARG$^{-/-}$ cells were grown in DMEM/F12-containing GlutaMAX (Gibco) and supplemented with 10% FBS and 1% penicillin–streptomycin. All cells were cultured in an incubator maintained at 37°C, 5% CO2, and a relative humidity of 95%.

Antibodies. All the antibodies used in this study are listed in *SI Appendix*, Table S5.

PDO and PDXO Generation and Growth Conditions. Written informed consent was obtained from all patients involved in the study. PDOs and PDXOs were grown according to the protocol described previously (22). The assembly of patient data, ovarian cancer tissues, ascites, and the pleural effusion fluids was implemented at the Dana-Farber Brigham Cancer Center under an Institutional Review Board (IRB)-approved protocol (02-051) under the Dana-Farber/Harvard Cancer Center IRB in conformity with the Declaration of Helsinki and Belmont Report. Detailed protocol for tissue and Ascites Processing for Patient Derived Organoids is described in SI appendix.

Survival Assays.

Clonogenic assay. Cells were counted and plated in triplicates in 6-well plates for colony formation assays. After 24 h, PARGi (PDD00017273) was added at various concentrations and the cells were incubated for 10 to 15 d. Further, cells were fixed with methanol for 10 min at room temperature, and then stained with crystal violet. Cell growth area quantification and imaging of the plates were performed with GelCount (Oxford Optronix).

3D cell viability assay for ovarian cancer PDOs and PDXOs. Cell Titer-Glo® 3D Cell Viability Assay was performed for drug sensitivity in isolated patient cells, ascites cells or PDX tumor cells. Detailed protocol for 3D Viability assay is described in SI appendix.

DNA fiber assay with S1 nuclease. To detect post replicative ssDNA gaps, we use a modified DNA fiber assay with ssDNA-specific enzyme S1 nuclease (22, 30, 47). In the presence of ssGAPs, S1 nuclease will nick the ssDNA opposite to the gap, thereby converting the ssDNA gap into a double-strand break which is then measured by the

shortening of IdU(5-Iodo-2′-Deoxyuridine) tracts. Briefly, cells were labeled with CldU (5-Chloro-2′-deoxyuridine) (Sigma Cat# C6891) for 30 min followed by IdU (Sigma Cat# I7125) for 2 h. PARGi was concomitantly added to the IdU labeling. Cells were further washed with PBS and permeabilized with CSK buffer(NaCl 100mM, MOPS 10mM, $MgCl_2$ 3mM, Sucrose 300mM, Triton X-100 0.5%) for 10 min. CSK buffer was washed away and S1 nuclease buffer added with or without S1 nuclease for 30 mins at 37 °C. Fiber assay was performed as per FiberPrep DNA extraction protocol (Genomic Vision, cat# EXT001A). Detailed protocol for the DNA fiber assay is described in SI appendix.

Immunofluorescence: S Phase PAR Assay. Cells were cultured on coverslips and treated with indicated drug or DMSO for 2 h. Cells were labeled with EdU for the last 15 min of treatment time. Cells were pre-extracted with 0.5% Triton X-100 for 5 mins, after which they were fixed with 4% paraformaldehyde for 10 min at RT. Cells were subsequently permeabilized in ice-cold methanol solution for 5 min. Further, cells were washed with PBS (3 × 5 min) and blocked with 3% BSA in 0.1% Triton X-100. EdU detection was performed using Click-iT EdU Alexa Fluor 488 Imaging Kit (Invitrogen Cat# C10337) according to the manufacturer's instructions. After click reaction, coverslips were washed with PBS (3 × 5 min) and stained for PAR/pADPr. Detailed protocol for immunofluorescence is described in SI appendix.

Quantification and Statistical Analysis. Quantitative data were analyzed and graphed using GraphPad Prism 9 or 10 software. All data are represented as median or mean with SEM. Significance was tested using the Mann–Whitney test. Assessment of synergy was calculated based on the Bliss model of synergy using Combenefit software (74).

Data, Materials, and Software Availability. All study data are included in the article and/or *SI Appendix*. Further information and requests for resources and reagents should be directed to and will be fulfilled by Lead Contact. Additional methods are described in *SI Appendix*. The RNA-seq datasets discussed in this publication have been deposited in NCBI tracking system #24694520 and are accessible through GEO Series accession GSE270384 (75).

ACKNOWLEDGMENTS. We would like to thank the generous patients who donated tissue for this work. We thank members of the D'Andrea laboratory for their helpful suggestions and comments. This work was supported by Sponsored Research Agreement funding from Bristol Myers Squibb (A.D.D. and G.I.S.), U.S. NIH grants (R01HL052725 and P01HL048546), the US Department of Defense (BM110181), the Breast Cancer Research Foundation, the Fanconi Anemia Research Fund, the Ludwig Center at Harvard, and the Smith Family Foundation (A.D.D.). This work was also supported by U.S. NIH grants P50 CA168504 (A.D.D. and G.I.S.) and P50 CA240243 (A.D.D. and G.I.S.).

Author affiliations: [a]Center for DNA Damage and Repair, Dana-Farber Cancer Institute, Boston, MA 02215; [b]Department of Radiation Oncology, Dana-Farber Cancer Institute, Boston, MA 02215; and [c]Department of Medical Oncology, Dana-Farber Cancer Institute, Boston, MA 02215

Author contributions: R.R., K.P., G.I.S., and A.D.D. designed research; R.R., O.S., A.A.B.A.d.C., S.M., and B.P.L., performed research; R.R., O.S., A.A.B.A.d.C., and H.N. analyzed data; C.G. help perform experiment; Y.J. help perform experiments; J.L. help get patient samples; B.K. help perform research; and R.R., K.P., G.I.S., and A.D.D. wrote the paper.

Reviewers: G.M., Penn State Milton S. Hershey Medical Center; and R.W.S., Brown University.

1. B. A. Gibson, W. L. Kraus, New insights into the molecular and cellular functions of poly(ADP-ribose) and PARPs. *Nat. Rev. Mol. Cell Biol.* **13**, 411–424 (2012).
2. R. Gupte, Z. Liu, W. L. Kraus, PARPs and ADP-ribosylation: Recent advances linking molecular functions to biological outcomes. *Genes. Dev.* **31**, 101–126 (2017).
3. A. Ray Chaudhuri, A. Nussenzweig, The multifaceted roles of PARP1 in DNA repair and chromatin remodelling. *Nat. Rev. Mol. Cell Biol.* **18**, 610–621 (2017).
4. M. A. Kassab, X. Yu, The role of dePARylation in DNA damage repair and cancer suppression. *DNA Repair (Amst.)* **76**, 20–29 (2019).
5. A. E. Fisher, H. Hochegger, S. Takeda, K. W. Caldecott, Poly(ADP-ribose) polymerase 1 accelerates single-strand break repair in concert with poly(ADP-ribose) glycohydrolase. *Mol. Cell Biol.* **27**, 5597–5605 (2007).
6. A. Ray Chaudhuri, A. K. Ahuja, R. Herrador, M. Lopes, Poly(ADP-ribosyl) glycohydrolase prevents the accumulation of unusual replication structures during unperturbed S phase. *Mol. Cell Biol.* **35**, 856–865 (2015).
7. D. Slade, PARP and PARG inhibitors in cancer treatment. *Genes. Dev.* **34**, 360–394 (2020).
8. S. H. Chen, X. Yu, Targeting dePARylation selectively suppresses DNA repair-defective and PARP inhibitor-resistant malignancies. *Sci. Adv.* **5**, eaav4340 (2019).
9. P. Gravells, E. Grant, K. M. Smith, D. I. James, H. E. Bryant, Specific killing of DNA damage-response deficient cells with inhibitors of poly(ADP-ribose) glycohydrolase. *DNA Repair (Amst.)* **52**, 81–91 (2017).
10. H. Fujihara *et al.*, Poly(ADP-ribose) Glycohydrolase deficiency sensitizes mouse ES cells to DNA damaging agents. *Curr. Cancer Drug Targets* **9**, 953–962 (2009).
11. H. Nagashima *et al.*, Poly(ADP-ribose) glycohydrolase inhibition sequesters NAD(+) to potentiate the metabolic lethality of alkylating chemotherapy in IDH-mutant tumor cells. *Cancer Discov.* **10**, 1672–1689 (2020).
12. H. E. Bryant *et al.*, Specific killing of BRCA2-deficient tumours with inhibitors of poly(ADP-ribose) polymerase. *Nature* **434**, 913–917 (2005).
13. H. Farmer *et al.*, Targeting the DNA repair defect in BRCA mutant cells as a therapeutic strategy. *Nature* **434**, 917–921 (2005).
14. K. Moore *et al.*, Maintenance olaparib in patients with newly diagnosed advanced ovarian cancer. *N. Engl. J. Med.* **379**, 2495–2505 (2018).
15. D. M. O'Malley, T. C. Krivak, N. Kabil, J. Munley, K. N. Moore, PARP inhibitors in ovarian cancer: A review. *Target Oncol.* **18**, 471–503 (2023).
16. K. Cong *et al.*, Replication gaps are a key determinant of PARP inhibitor synthetic lethality with BRCA deficiency. *Mol. Cell* **81**, 3227 (2021).
17. M. P. Dias, S. C. Moser, S. Ganesan, J. Jonkers, Understanding and overcoming resistance to PARP inhibitors in cancer therapy. *Nat. Rev. Clin. Oncol.* **18**, 773–791 (2021).
18. S. Saxena, L. Zou, Hallmarks of DNA replication stress. *Mol. Cell* **82**, 2298–2314 (2022).
19. K. Cong, S. B. Cantor, Exploiting replication gaps for cancer therapy. *Mol. Cell* **82**, 2363–2369 (2022).
20. A. Taglialatela *et al.*, REV1-Polzeta maintains the viability of homologous recombination-deficient cancer cells through mutagenic repair of PRIMPOL-dependent ssDNA gaps. *Mol. Cell* **81**, 4008–4025 e4007 (2021).
21. A. Quinet, S. Tirman, E. Cybulla, A. Meroni, A. Vindigni, To skip or not to skip: Choosing repriming to tolerate DNA damage. *Mol. Cell* **81**, 649–658 (2021).
22. A. da Costa *et al.*, Single-stranded DNA gap accumulation is a functional biomarker for USP1 inhibitor sensitivity. *Cancer Res.* **84**, 3435–3446 (2024). 10.1158/0008-5472.CAN-23-4007.
23. J. B. Khatib, C. M. Nicolae, G. L. Moldovan, Role of Translesion DNA Synthesis in the Metabolism of Replication-associated Nascent Strand Gaps. *J. Mol. Biol.* **436**, 168275 (2024).
24. A. Quinet *et al.*, PRIMPOL-mediated adaptive response suppresses replication fork reversal in BRCA-deficient cells. *Mol. Cell* **77**, 461–474 e469 (2020).
25. S. Tirman *et al.*, Temporally distinct post-replicative repair mechanisms fill PRIMPOL-dependent ssDNA gaps in human cells. *Mol. Cell* **81**, 4026–4040.e8 (2021).
26. A. Simoneau, R. Xiong, L. Zou, The trans cell cycle effects of PARP inhibitors underlie their selectivity toward BRCA1/2-deficient cells. *Genes. Dev.* **35**, 1271–1289 (2021).
27. A. Schreuder, T. J. Wendel, C. G. V. Dorresteijn, S. M. Noordermeer, Single-stranded DNA) gaps in understanding BRCAness. *Trends Genet.* **40**, 757–771 (2024). 10.1016/j.tig.2024.04.013.
28. O. Belan *et al.*, POLQ seals post-replicative ssDNA gaps to maintain genome stability in BRCA-deficient cancer cells. *Mol. Cell* **82**, 4664–4680.e9 (2022).
29. A. Schrempf *et al.*, POLtheta processes ssDNA gaps and promotes replication fork progression in BRCA1-deficient cells. *Cell Rep.* **41**, 111716 (2022).
30. A. Syed *et al.*, Novobiocin blocks nucleic acid binding to Poltheta and inhibits stimulation of its ATPase activity. *Nucleic Acids Res.* **51**, 9920–9937 (2023).
31. M. Paes Dias *et al.*, Loss of nuclear DNA ligase III reverts PARP inhibitor resistance in BRCA1/53BP1 double-deficient cells by exposing ssDNA gaps. *Mol. Cell* **81**, 4692–4708.e9 (2021).
32. E. Guo *et al.*, FEN1 endonuclease as a therapeutic target for human cancers with defects in homologous recombination. *Proc. Natl. Acad. Sci. U.S.A.* **117**, 19415–19424 (2020).
33. T. Kaufmann *et al.*, A novel non-canonical PIP-box mediates PARG interaction with PCNA. *Nucleic Acids Res.* **45**, 9741–9759 (2017).
34. O. Mortusewicz, E. Fouquerel, J. C. Ame, H. Leonhardt, V. Schreiber, PARG is recruited to DNA damage sites through poly(ADP-ribose)- and PCNA-dependent mechanisms. *Nucleic Acids Res.* **39**, 5045–5056 (2011).
35. N. Pillay, R. M. Brady, M. Dey, R. D. Morgan, S. S. Taylor, DNA replication stress and emerging prospects for PARG inhibitors in ovarian cancer therapy. *Prog. Biophys. Mol. Biol.* **163**, 160–170 (2021).
36. N. Pillay *et al.*, DNA replication vulnerabilities render ovarian cancer cells sensitive to poly(ADP-Ribose) glycohydrolase inhibitors. *Cancer Cell* **35**, 519–533.e8 (2019).
37. H. Dungrawala *et al.*, The replication checkpoint prevents two types of fork collapse without regulating replisome stability. *Mol. Cell* **59**, 998–1010 (2015).
38. J. H. Houl *et al.*, Selective small molecule PARG inhibitor causes replication fork stalling and cancer cell death. *Nat. Commun.* **10**, 5654 (2019).
39. H. Hanzlikova *et al.*, The importance of poly(ADP-Ribose) Polymerase as a sensor of unligated okazaki fragments during DNA replication. *Mol. Cell* **71**, 319–331.e3 (2018).
40. C. Coulson-Gilmer *et al.*, Replication catastrophe is responsible for intrinsic PAR glycohydrolase inhibitor-sensitivity in patient-derived ovarian cancer models. *J. Exp. Clin. Cancer Res.* **40**, 323 (2021).
41. C. Andronikou *et al.*, PARG-deficient tumor cells have an increased dependence on EXO1/FEN1-mediated DNA repair. *EMBO J.* **43**, 1015–1042 (2024).
42. D. I. James *et al.*, First-in-class chemical probes against poly(ADP-ribose) glycohydrolase (PARG) inhibit DNA repair with differential pharmacology to olaparib. *ACS Chem. Biol.* **11**, 3179–3190 (2016).
43. A. Tsherniak *et al.*, Defining a cancer dependency map. *Cell* **170**, 564–576.e516 (2017).
44. T. Thakar *et al.*, Ubiquitinated-PCNA protects replication forks from DNA2-mediated degradation by regulating Okazaki fragment maturation and chromatin assembly. *Nat. Commun.* **11**, 2147 (2020).
45. H. Sun *et al.*, Okazaki fragment maturation: DNA flap dynamics for cell proliferation and survival. *Trends Cell Biol.* **33**, 221–234 (2023).
46. L. Nie *et al.*, DePARylation is critical for S phase progression and cell survival. *eLife* **12**, RP89303 (2024).
47. A. Quinet, D. Carvajal-Maldonado, D. Lemacon, A. Vindigni, DNA fiber analysis: Mind the gap! *Methods Enzymol* **591**, 55–82 (2017).
48. S. Roy, J. W. Luzwick, K. Schlacher, SIRF: Quantitative in situ analysis of protein interactions at DNA replication forks. *J. Cell Biol.* **217**, 1521–1536 (2018).

49. K. H. Leung, M. Abou El Hassan, R. Bremner, A rapid and efficient method to purify proteins at replication forks under native conditions. *Biotechniques* **55**, 204–206 (2013).
50. S. Jungmichel *et al.*, Proteome-wide identification of poly(ADP-Ribosyl)ation targets in different genotoxic stress responses. *Mol. Cell* **52**, 272–285 (2013).
51. M. C. Haigis *et al.*, SIRT4 inhibits glutamate dehydrogenase and opposes the effects of calorie restriction in pancreatic beta cells. *Cell* **126**, 941–954 (2006).
52. R. E. London, XRCC1 – Strategies for coordinating and assembling a versatile DNA damage response. *DNA Repair (Amst.)* **93**, 102917 (2020).
53. J. Li *et al.*, NAD(+) bioavailability mediates PARG inhibition-induced replication arrest, intra S-phase checkpoint and apoptosis in glioma stem cells. *NAR Cancer* **3**, zcab044 (2021).
54. A. Dhoonmoon, C. M. Nicolae, G. L. Moldovan, The KU-PARP14 axis differentially regulates DNA resection at stalled replication forks by MRE11 and EXO1. *Nat. Commun.* **13**, 5063 (2022).
55. A. Hale, A. Dhoonmoon, J. Straka, C. M. Nicolae, G. L. Moldovan, Multi-step processing of replication stress-derived nascent strand DNA gaps by MRE11 and EXO1 nucleases. *Nat. Commun.* **14**, 6265 (2023).
56. L. G. Bennett *et al.*, MRNIP limits ssDNA gaps during replication stress. *Nucleic Acids Res.* **52**, 8320–8331 (2024).
57. W. C. Burhans *et al.*, Emetine allows identification of origins of mammalian DNA replication by imbalanced DNA synthesis, not through conservative nucleosome segregation. *EMBO J.* **10**, 4351–4360 (1991).
58. D. Lukac, Z. Machacova, P. Moudry, Emetine blocks DNA replication via proteosynthesis inhibition not by targeting Okazaki fragments. *Life Sci. Alliance* **5**, e202201560 (2022).
59. S. Tirman, E. Cybulla, A. Quinet, A. Meroni, A. Vindigni, PRIMPOL ready, set, reprime! *Crit. Rev. Biochem. Mol. Biol.* **56**, 17–30 (2021).
60. A. S. Kawale *et al.*, APOBEC3A induces DNA gaps through PRIMPOL and confers gap-associated therapeutic vulnerability. *Sci. Adv.* **10**, eadk2771 (2024).
61. S. J. Hill *et al.*, Prediction of DNA repair inhibitor response in short-term patient-derived ovarian cancer organoids. *Cancer Discov.* **8**, 1404–1421 (2018).
62. O. Kopper *et al.*, An organoid platform for ovarian cancer captures intra- and interpatient heterogeneity. *Nat. Med.* **25**, 838–849 (2019).
63. S. Bose, H. Clevers, X. Shen, Promises and challenges of organoid-guided precision medicine. *Med.* **2**, 1011–1026 (2021).
64. E. H. Stover, K. Fuh, P. A. Konstantinopoulos, U. A. Matulonis, J. F. Liu, Clinical assays for assessment of homologous recombination DNA repair deficiency. *Gynecol. Oncol.* **159**, 887–898 (2020).
65. K. Parmar *et al.*, The CHK1 inhibitor prexasertib exhibits monotherapy activity in high-grade serous ovarian cancer models and sensitizes to PARP inhibition. *Clin. Cancer Res.* **25**, 6127–6140 (2019).
66. W. Min *et al.*, Poly(ADP-ribose) binding to Chk1 at stalled replication forks is required for S-phase checkpoint activation. *Nat. Commun.* **4**, 2993 (2013).
67. G. Acharya *et al.*, CHK1 inhibitor induced PARylation by targeting PARG causes excessive replication and metabolic stress and overcomes chemoresistance in ovarian cancer. *Cell Death Discov.* **10**, 278 (2024).
68. W. Leung *et al.*, ATR protects ongoing and newly assembled DNA replication forks through distinct mechanisms. *Cell Rep.* **42**, 112792 (2023).
69. J. Ledermann *et al.*, Olaparib maintenance therapy in platinum-sensitive relapsed ovarian cancer. *N. Engl. J. Med.* **366**, 1382–1392 (2012).
70. R. L. Coleman *et al.*, Rucaparib maintenance treatment for recurrent ovarian carcinoma after response to platinum therapy (ARIEL3): A randomised, double-blind, placebo-controlled, phase 3 trial. *Lancet* **390**, 1949–1961 (2017).
71. M. R. Mirza *et al.*, Niraparib maintenance therapy in platinum-sensitive, recurrent ovarian cancer. *N. Engl. J. Med.* **375**, 2154–2164 (2016).
72. A. Mann *et al.*, POLtheta prevents MRE11-NBS1-CtIP-dependent fork breakage in the absence of BRCA2/RAD51 by filling lagging-strand gaps. *Mol. Cell* **82**, 4218–4231.e8 (2022).
73. D. Harrision, P. Gravells, R. Thompson, H. E. Bryant, Poly(ADP-Ribose) glycohydrolase (PARG) vs. poly(ADP-ribose) polymerase (PARP)–Function in genome maintenance and relevance of inhibitors for anti-cancer therapy. *Front. Mol. Biosci.* **7**, 191 (2020).
74. G. Y. Di Veroli *et al.*, Combenefit: An interactive platform for the analysis and visualization of drug combinations. *Bioinformatics* **32**, 2866–2868 (2016).
75. R. Ravindranathan, K. Parmar, H. Nguyen, A. D. D'Andrea, PARG inhibitor sensitivity correlates with accumulation of single strand DNA gaps in preclinical models of ovarian cancer. Gene Expression Omnibus. https://www.ncbi.nlm.nih.gov/geo/query/acc.cgi?acc=GSE270384. Deposited 20 June 2024.